spectral range, but with a concomitant lower resolution, had to be used. The central portion of the spectrum was recorded by tilting a high-resolution Fabry-Perot with a 5-cm plate spacing. The experimental resolution, corresponding to a full width at half-maximum of 150 MHz, is largely determined by the short pulse duration of 4×10^{-9} sec, in accordance with the uncertainty principle. Unfortunately this resolution is not sufficient to resolve all of the individual components.

In this context it should be noted that the nitrogen-laser–pumped dye laser available to us was designed for high peak power output and intended for the investigation of nonlinear optical properties of crystals and liquids. Hänsch has shown that much higher resolution of about 10 MHz can be obtained with cw dye lasers. The nonlinearity of many two-photon transitions in alkali vapors is so large that a focused beam with 0.1–1-W cw power is sufficient for their observation. Our limited resolution was, however, sufficient to obtain confirmation of the rather striking selection rules and Zeeman splittings governing two-photon transitions between one-electron ^2S states.

*Research supported by the Joint Services Electronics Program.

[1]M. D. Levenson and N. Bloembergen, Phys. Rev. Lett. 32, 645 (1974).

[2]F. Biraben, B. Cagnac, and G. Grynberg, Phys. Rev. Lett. 32, 643 (1974).

[3]T. W. Hänsch, K. C. Harvey, G. Meisel, and A. L. Schawlow, to be published.

[4]L. S. Vasilenko, V. P. Chebotenev, and A. V. Shishaev, Pis'ma Zh. Eksp. Teor. Fiz. 12, 161 (1970) [JETP Lett. 12, 113 (1970)].

[5]B. Cagnac, G. Grynberg, and F. Biraben, J. Phys. (Paris) 34, 845 (1973).

[6]A. Rosen and I. Lindgren, Phys. Scr. 6, 109 (1972).

Raman Scattering from Vibronic Levels of a Jahn-Teller–Distorted Complex*

S. Guha and L. L. Chase†
Indiana University, Bloomington, Indiana 47401
(Received 6 March 1974)

Raman-scattering transitions have been observed between the hindered rotational states of the Jahn-Teller–distorted ^2E_g ground state of Cu^{2+} in CaO. Impurity-induced scattering from the CaO vibrations was also observed. The results are in good agreement with the cluster model for the low-lying vibronic states.

The vibronic energy levels of Jahn-Teller–distorted impurity complexes in solids have been the subject of many theoretical efforts over the previous two decades. However, no unambiguous and extensive experimental information has been obtained in this area because of the lack of a spectroscopic technique which was not limited severely by frequency range, selection rules, or complications resulting from extraneous spectral information not related to the Jahn-Teller distortion. We report the first observation of Raman scattering from both the hindered rotational levels and the impurity-perturbed lattice vibrations associated with a Jahn-Teller distortion. The experiments were performed on the ^2E_g electronic ground state of the Cu^{2+} ion at a Ca site in CaO. The substantial intensity of the spectra, particularly for the transitions between the rotational levels, suggests that this will be a powerful and widely applicable method for studying the Jahn-Teller effect.

The experiments were performed using the 5154-Å argon laser line and conventional photon-counting detection techniques. An I_2 filter[1] was employed for the work within 200 cm^{-1} of the laser line to reduce the intensity of the Rayleigh-scattered laser light. The samples were grown at Oak Ridge National Laboratory by an arc-fusion method and had varying Cu^{2+} concentrations from sample to sample as well as over the volume of each sample. Spectra were obtained for polarization geometries for which the E_g, $E_g + A_{1g}$, and T_{2g} scattering symmetries were observed.

The E_g spectrum at 4.2°K for the 0–200-cm^{-1} region is shown in Fig. 1. Four sharp lines are observed at 4, 26, 34, and 38.5 cm^{-1}. In addition, three broader and weaker peaks appear at

about 65, 105, and ~180 cm^{-1}. The inset of Fig. 1 is an expanded low-frequency spectrum to show the 4-cm^{-1} transition more clearly. With the 200-mW power level of the laser in single-mode operation and the ~60% absorption of the I_2 filter, the intensities of the peaks in Fig. 1 correspond to about 500 photocounts/sec. The $E_g + A_{1g}$ spectrum is identical to the E_g spectrum to within the experimental accuracy, and no scattering is observed in the T_{2g} geometry below 200 cm^{-1}. At 77°K, the rotational spectrum is broadened so that the three transitions between 26 and 38.5 cm^{-1} appear as a single broad peak.

The energy levels of the coupled electronic-vibrational Hamiltonian for a doubly degenerate electronic state interacting with a doubly degenerate molecular vibration were calculated for linear coupling by Longuet-Higgins *et al.*[2] and were subsequently extended by O'Brien[3] to include the effects of anharmonicity. For strong coupling, the lowest energy levels correspond to a hindered rotation of the distorted complex between equivalent minima of the effective nuclear potential. These minima correspond to tetragonal distortions along the cube axes of the neighboring oxygens for the Cu^{2+} ion in the CaO lattice. The parameters which characterize the hindered-rotational levels are the rotational splitting and the height of the potential barrier, 2β, between the minima. The rotational splitting is[3]

$$E(j) = (\hbar^2/2\mu\rho_0^2)(j^2 + \tfrac{1}{4}) = \alpha(j^2 + \tfrac{1}{4}), \qquad (1)$$

where ρ_0 is related to the amplitude of the distortion, j is a half-odd-integral rotational quantum number, and μ is the effective mass associated with the vibrational motion. The resulting energy levels are linear combinations of the rotational levels and are either singly or doubly degenerate. They transform as the A_{1g}, A_{2g}, or E_g representations of O_h. The group-theoretical selection rules for Raman transitions between these states are that the $A_1 \leftrightarrow E$, $A_2 \leftrightarrow E$, and $E \leftrightarrow E$ transitions are allowed in E_g scattering and the $A_1 \leftrightarrow A_1$, $A_2 \leftrightarrow A_2$, and $E \leftrightarrow E$ transitions are allowed in A_{1g}. The $A_1 \leftrightarrow A_2$ transitions are forbidden, and no scattering is allowed in the T_{2g} geometry.

We have fitted the data of Fig. 1 with the eigenvalue plots of O'Brien,[3] and find a quite satisfactory agreement with the energies of the six lowest excited levels, A_{1g}, A_{2g}, E_g, E_g, $A_{1g}+A_{2g}$, and E_g, above the E_g ground state. The parameters obtained from the fit are $\alpha = 5$ cm^{-1} and $2\beta = 43$ cm^{-1}. The measured and calculated energies (in cm^{-1}) are (calculated values in parentheses), for A_{1g}, 4 (3.8); A_{2g}, 26 (26.5); E_g, 38.5 (38); E_g, 65 (63.5); $A_{1g}+A_{2g}$, 105 (99); E_g, 180 (145). Since no A_{1g} scattering was observable, the selection rules were only of use in identifying a missing transition as $A_1 \leftrightarrow A_2$, and we were further guided by the results of electron-spin-resonance measurements[4] to give the sign of the stabilized distortion which gives A_{1g} as the lowest excited state. The identification of the level at 180 cm^{-1} is somewhat uncertain since it is close enough to the 200-cm^{-1} zone-boundary acoustic peak of CaO in Fig. 2 that it could also result from the perturbed lattice vibrational spectrum. The abrupt decrease in intensity of the spectra beyond the 38.5-cm^{-1} transition is qualitatively consistent with the small value of β/α and the selection rules for Raman scattering in the pure rotational limit.[5]

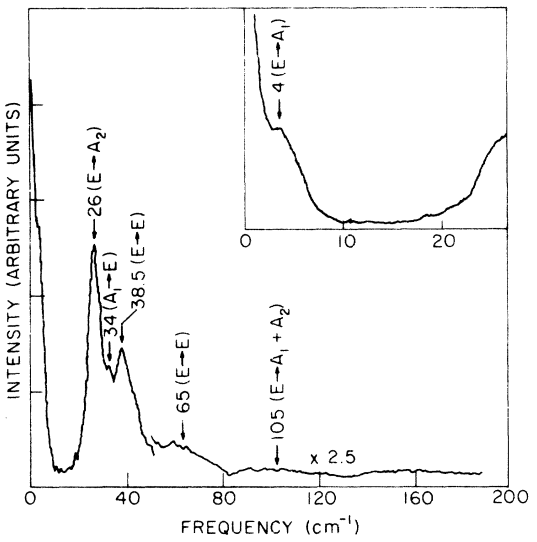

FIG. 1. The hindered rotational spectrum of CaO:Cu^{2+}. Note the scale change of 2.5 for frequency shifts > 50 cm^{-1}. The inset at the upper right shows an expanded low-frequency spectrum containing the ~4 cm^{-1} $E \rightarrow A_1$ transition.

The good agreement with the molecular cluster model is remarkable since the electronic state is coupled not to a single degenerate vibration, but to most of the lattice vibrations of CaO. Some theoretical approaches to this problem have been proposed recently,[6-9] and the work of O'Brien[7] shows that the rotational energy levels for strong coupling, neglecting anharmonicity, still have the form of Eq. (1), but with a value of α reduced

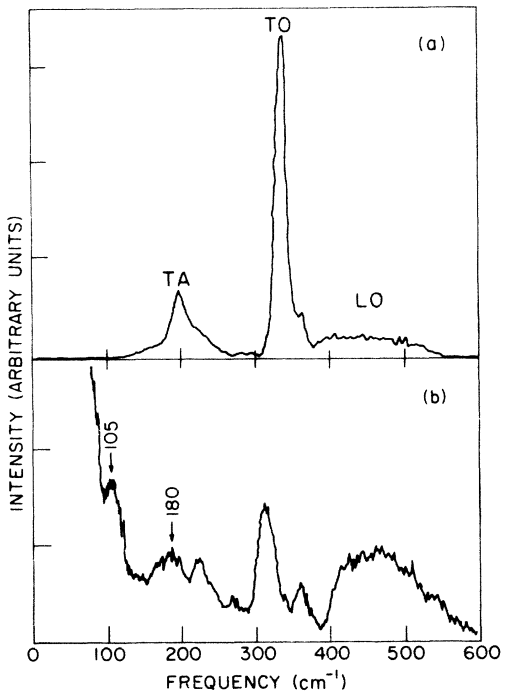

FIG. 2. The (a) calculated and (b) measured impurity-induced vibrational spectra of CaO:Cu^{2+}. The CaO vibrational branches giving the largest contributions to the calculated intensities are designated in (a). The 105- and 180-cm^{-1} rotational transitions are labeled in (b) for a comparison of the intensities of the rotational and lattice-mode scattering.

by the coupling to a phonon continuum. An important assumption of these recent theories is that $\langle \Delta\omega^2 \rangle \ll \omega_{\text{eff}}^2$, where $\langle \Delta\omega^2 \rangle$ is the mean square spread in frequencies to which the electronic state is coupled and ω_{eff} is a weighted-average frequency.[7] This aspect of the problem can also be examined by Raman-scattering methods. In Fig. 2 is shown the impurity-induced, lattice-vibrational E_g-symmetry scattering at 77°K. This spectrum was obtained without filtering using a double monochromator, which results in a large Rayleigh-scattered intensity out to 100 cm^{-1}. The two-phonon spectrum of CaO, measured in a pure CaO sample, has been subtracted from the data.

The scattering spectrum expected for an isotopic impurity has been calculated assuming coupling to only the nearest-neighbor oxygen ions. Shell-model lattice dynamics, with parameters obtained from neutron scattering data at 300°K,[10] were used to obtain the projected density of states for E_g distortions of the oxygen octahedron, which is plotted in Fig. 2. Although the prominent features are qualitatively similar to the data, there are pronounced differences in the positions and relative intensities of most of them. Data taken at 300°K are not markedly different from those at 77°K so that the differences do not result from changes with temperature. Perhaps the most important of these differences is the large integrated scattering intensity observed in the 400–500-cm^{-1} region of the LO modes in CaO. Data will be required for similar scattering from an orbital singlet impurity of the same size as Cu^{2+} to determine if these differences result from its small size compared with the Ca^{2+} or from the Jahn-Teller distortion. In either case, it is clear from the data that the assumption concerning the frequency spread of the vibronic coupling is not well satisfied in this case.

In the cluster model, the rotational splitting factor α is related to the stabilization energy E_{JT} for the distorted complex by

$$E_{JT} = (\hbar\omega_{\text{eff}})^2/4\alpha. \quad (2)$$

Both the data and calculated spectrum in Fig. 2 suggest a value of $\hbar\omega_{\text{eff}} \sim 350$ cm^{-1}. We find the corrections to α given in Eq. (44) of Ref. 6 to be $< 10\%$, and, from $\alpha = 5$ cm^{-1}, we obtain $E_{JT} \cong 6000$ cm^{-1}. This is most likely to be an overestimate of E_{JT}, since the ω_{eff}^2 factor enters Eq. (2) because of its proportionality to the effective force constant for E_g distortions of the oxygen neighbors. Because of the small size of Cu^{2+}, this force constant may be somewhat smaller than the $\mu\omega_{\text{eff}}^2$ estimated from the lattice-mode scattering distribution of Fig. 2. Strong Raman scattering is also expected between the two sheets of the effective potential surface,[10] which would have a maximum intensity at $\Delta E \sim 4E_{JT}$ and could therefore determine E_{JT} directly. Although some polarized scattering is observed at large frequency shifts in this case, the large E_{JT} would place the peak outside the range of our detection system. Also, fluorescence from impurities is also present in our samples at large shifts, which complicates the observation of this scattering.

We are grateful to Dr. Marvin Abraham and Dr. Yok Chen of Oak Ridge National Laboratory for allowing us to use their excellent CaO samples for these experiments.

*Work supported by the National Science Foundation under Grant No. GH33404.

†Alfred P. Sloan Foundation Fellow.

[1]G. E. Devlin, J. L. Davis, L. L. Chase, and S. Geschwind, Appl. Phys. Lett. 19, 138 (1971).
[2]H. C. Longuet-Higgins, U. Opik, M. H. L. Pryce, and R. A. Sack, Proc. Roy. Soc., Ser. A 244, 1 (1958).
[3]M. C. M. O'Brien, Proc. Roy. Soc., Ser. A 281, 323 (1964).
[4]L. A. Boatner, R. W. Reynolds, M. Abraham, and Y. Chen, to be published.
[5]M. S. Child and H. C. Longuet-Higgins, Phil. Trans. Roy. Soc. London, Ser. A 254, 259 (1962).
[6]J. R. Fletcher, J. Phys. C: Proc. Phys. Soc., London 5, 852 (1972).
[7]M. C. M. O'Brien, J. Phys. C: Proc. Phys. Soc., London 5, 2045 (1972).
[8]R. Englman and B. Halperin, J. Phys. C: Proc. Phys. Soc., London 6, L219 (1973).
[9]N. Gauthier and M. B. Walker, Phys. Rev. Lett. 31, 1211 (1973).
[10]D. H. Saunderson and G. E. Peckham, J. Phys. C: Proc. Phys. Soc., London 4, 2009 (1971).

Determination of the Electron Thermal Conductivity across Magnetic Surfaces in the FM-1 Spherator*

S. Ejima, M. Okabayashi, and J. Schmidt
Plasma Physics Laboratory, Princeton University, Princeton, New Jersey 08540
(Received 17 December 1973)

A new approach was taken to measure the electron thermal conductivity across magnetic surfaces by utilizing localized upper hybrid resonance heating. The electron thermal conductivity coefficient measured in the FM-1 spherator was increased with an increase of electron temperature for $T_e > 1$ eV. The dependence is similar to that of the particle diffusion coefficient. The absolute value was 10–20 times smaller than the Bohm coefficient.

The thermal conductivity across magnetic surfaces in toroidal devices has been studied experimentally by many groups in an effort to understand the mechanisms responsible for the transport. In many cases the average thermal transport has been determined from the energy balance.[1,2] A new approach is reported in this paper to measure locally the electron thermal conductivity across the magnetic surfaces by utilizing localized upper hybrid resonance heating. The electron thermal conductivity measured in the FM-1 spherator with this new method was found to be anomalous. The electron thermal conductivity increases with an increase of electron temperature; this dependence is similar to that of the particle diffusion coefficient. The absolute value of the electron thermal conductivity was 10^{-1}–5×10^{-2} of the one estimated from the Bohm coefficient. Within our best knowledge, the present report is the first direct observation of local electron thermal conductivity across the magnetic surfaces in toroidal devices.

As is well known,[3] microwave power with a frequency $\omega_0/2\pi$ close to the electron-cyclotron frequency $\omega_{ce}/2\pi$ is absorbed in a localized area which satisfies the upper hybrid resonance condition, $\omega_r^2(\psi,\chi) \equiv \omega_{pe}^2(\psi) + \omega_{ce}^2(\psi,\chi)$, where $\omega_{pe}/2\pi$ is the electron plasma frequency and (ψ,χ,θ) are the toroidal coordinates. At the resonance the energy is mainly deposited in the electrons with mild ion heating.[3] Although the localized resonance $\omega_r = \omega_0$ does not coincide with a magnetic surface, the strong energy absorption takes place on a magnetic surface which is tangential to the resonance surface. By reducing the pulse width of the resonant heating, it is possible to localize the heating around the maximum energy absorption surface. The pulse length should be long enough to allow the heat to spread uniformly on the magnetic surface. The observed spreading of the initially localized heat after the termination of the heat pulse provides a measurement of the electron thermal conductivity across magnetic surfaces. In the present paper we report experimental results in the FM-1 spherator on (1) the production of a localized heat source and the observation of heat spreading, (2) the determination of the local electron thermal conductivity coefficient $K_\perp$, and (3) the determination of the dependence of $K_\perp$ on the electron temperature. The identification of the heating mechanism is described elsewhere.[3]

The FM-1 spherator[4] is a toroidal plasma confinement device which has a magnetically levitated superconducting ring inside the plasma confinement volume. The superconducting ring was